International Journal of Mathematics Trends and Technology
ISSN: 2231-5373/ https://doi.org/10.14445/22315373/IJMTT-V72I6P102
Volume 72 Issue 6, 7-23, June 2026

Original Article

Darcy-Forchheimer Stagnation Point Flow of a Maxwell Nanofluid Past A Rotating Disk With Cattaneo-Christov, Soret-Duffor and Active Energy Effects

Ch. Kishore Kumar

[1]*Department of Mathematics, Nizam Colleges(A), Osmania University, Hyderabad, India.*

Corresponding Author : kishoresai09@gmail.com

Received: 21 April 2026 Revised: 27 May 2026 Accepted: 14 June 2026 Published: 29 June 2026

Abstract *- The study is to investigate the stagnation point flow of a Maxwell Nanofluid. To make the present paper more realistic, the Cattaneo- Christove heat source effect was included. The theory of Cattaneo-Christov shows that the mass transport and heat mechanisms of the fluid can be improved by replacing Fick's and Fourier laws. The active energy was introduced to study more about the fluid nature. After examining the physical phenomena of the fluid flow, the governing equations(PDE'S) were constructed. The well-defined similarity transformations were used to convert the PDE's to a system of coupled ODE's. The Matlab-BVP4c is used to solve these ODE's. The results were interpreted through Graphs. It is observed that the velocity outline decreases as the Deborah number ϖ increases, and also it is noticed that a rise in the magnetic field decays the velocity profile.*

Keywords *- Maxwell Nanofluid, MHD, Cattaneo-Christov, Active energy, Thermo diffusion.*

1. Introduction

The 3-D viscous flow caused by rotating of a disk was done by Von Karman[1]. Later, this problem was subsequently extended through theoretical and experimentally by Cochran. [2], Goldstein [3] and Gregory *et al.,* [4]. Owing to the extensive applications of MHD in industrial and manufacturing processes, numerous studies have been conducted, both experimentally and theoretically, on flow over a rotating disk. The MHD flow past a rotating disk in a porous medium, along with Ohmic viscous dissipation & heating, was studied by Sibanda & Makinde [5]. The stagnation point flow of this program into a 2-D impinging on a flat wall by Hiemenz [6]. He considered the two-dimensional orthogonal flow over a flat plate for his research. Homann [7] later extended this work by including axisymmetric motion. Wang [8] came to the conclusion that it is observed that peak mass deposition, heat transfer, and pressure are attained within the stagnation zone.

The stagnation point flow of Burgers fluid with Newtonian heating was examined by Hayat et al., [9]. The Asymmetric stagnation point flow is characterized by a constant wall displacement, and it was presented by Agarwal [10]. Weidman [11] extended this concept to a rotating disk. In addition to that, the magnetic field's effect on the flow driven by the disc deformable nature was studied by Turkyilmazoglu [12]. The various parameters of the flow, like magnetic flow, stretchy variable, and rotatory parameter, are related to the stagnation velocities and shear stresses. The flow direction in a radial branch is a similar concept to that was done by Lok *et al.,* [13]. The micro-porous fluid stagnation point flow in a spinning disk was illustrated by Sajid [14]. According to Darcy's law, the fluid velocity in a porous medium is directly proportional to the applied pressure gradient. Henry Darcy founded the earth science discipline of hydrogeology. Later, his studies were utilized by Whitaker [15] by considering water movement across sand beds. Morris Muskat[16] explained the fundamental principle of how single-phase fluid passes through a porous medium. Hayat et al., [17] analyzed the unsteady Magnetohydrodynamic Darcy–Forchheimer flow of Nanofluids past a stretching surface. The thermophoresis diffusion, Brownian motion, and nonlinear mixed convection—which occurs during heat transmission—all contribute to the description of the characteristics of nano materials. The impact of the rotating disk-induced partial slip effect on the Darcian flow for CNT was examined by Sadiq *et al.,* [18]. The dual-diffusion Cattaneo–Christov model incorporating Darcy flow over an exponentially curved sheet was analyzed by Muhammad et al.,[19]. A similar work was extended by Haider [20] by considering the porous medium. Industrial and biomedical sectors are known to use heat transfer techniques. The concept is based on Continuum mechanics and Fourier's law, which provides a mechanism for transporting heat. However, this rule does not take into account the lag factor, which makes the model incredibly impractical. The researchers expanded upon this rule in subsequent years [21- 25] & the name of the Cattaneo-Christov heat flow model was changed to the CC model made

by [26]. Some of the noteworthy studies that investigated the flow characteristics of Nanofluids in co-axial disks were carried out using the CC model. Such as, Ziya *et al.,* [27] used titanium dioxide for their analysis. In another study, Noreen et al [28] used the Cattaneo Christov model to study how hybrid Nanofluids effected the double-spinned disks' performance.

The complex behavior of thermo-viscous fluid flow between horizontal porous stretched plates embedded in a porous medium was studied by N. Pothanna et.al., [29] using Artificial Neural Networks (ANNs). In this study, the governing equations for momentum and energy transport were formulated by incorporating the viscosity effects, the porous medium's resistance, and thermal conduction. The same work was extended by P. Nalimela, et.al.,[30] wherein they studied the unsteady fluid flow over a horizontal oscillating flat plate embedded within a porous slab. Kumar Singh and Verma studied the unsteady fluid flow around an oscillating sphere. Kumar *et.al*.,[31] investigated the MHD Casson fluid flow in a 2D Forchheimer porous medium over an inclined nonlinear surface. Similar works were done by [32]-[39]

After the careful observation of the above investigations, there is still a vacuum in the area of flow past a rotating disk. Hence, the present study gives a detailed analysis of Darcy-Forchheimer stagnation point flow of a Maxwell Nanofluid past a rotating disk with Cattaneo-Christov, Soret-Duffor, and active energy effects. Since the study includes the Cattaneo-Christov effect, it gives a detailed account of thermal relaxation effects and increases the speed of heat transfer.

2. Mathematical Formulation

The goal of this study is to analyze the axisymmetric stagnation point flow of a Maxwell Nanofluid through a spinning disk. The concept of the physical problem is presented by the use of cylindrical coordinates. The velocity components are defined in the radial (r), azimuthal (θ), and axial (z) directions. Assuming all physical quantities are independent of the azimuthal coordinate, that is, $\partial/\partial\theta = 0$The stagnation line is situated $at\ z < 0$, whereas the flow domain occupies the upper half-plane $(z \geq 0)$. It is presumed that the movement of the disk is radially aligned with its velocity. The movement of the disk is also characterized by a rotation rate that is greater than the rotational speed. It is widely believed that the temperature of the upper part of the spinning disk is higher than that of the surrounding fluid. The volume of nanoparticles in the free stream also has a higher value percentage. This study is carried out using a Nanofluid model developed by Bruno Buongiorno. The goal of this research is to explore the effect of nanoparticles on Brownian motion and thermophoresis of the Maxwell Nanofluid and added Cattaneo -Christov heat flux theory on spinning disk with the effect on Soret Dufour terms, in addition to this non uniform heat source/sink term was added. The results of the research are based on a mathematical model that presents various presumptions and requirements. The rotation of the disk $z = 0$ is also determined by its angular velocity. It is assumed that the disk's Axis of symmetry does not get affected by the movement of the tangential disk. Its component velocities are expressed by means of cylindrical coordinates (r, ϕ, z), and its radical expansions are assumed to be constant $u = cr$. The free stream velocity is expressed as $u_e = dr$, which includes the parameters d and r, which are relevant to the model. Finally, the temperature of the fluid T_f is taken into account to determine its properties.

Continuity Equation:

$$\left(\frac{1}{r}\right) * \frac{d}{dr}(r\,u) + d\frac{w}{d}z = 0 \quad [1]$$

Radial Momentum Equation:

$$u\frac{\partial u}{\partial r} + w\frac{\partial u}{\partial z} - \frac{v^2}{r} - u_e\frac{du_e}{dr} = \nu_f\nabla^2 u - \beta_1 M_r - \frac{\sigma B_0^2}{\rho_f}(u - u_e) - \frac{\nu}{k^*}(u - u_e) - F_r(u^2 - u_e^2) \quad [2]$$

Where $M_r = u^2\frac{\partial^2 u}{\partial r^2} + w^2\frac{\partial^2 u}{\partial z^2} + 2uw\ \frac{\partial^2 u}{\partial r\partial z} - \frac{2uv}{r}\frac{\partial v}{\partial r} - \frac{2vw}{r}\frac{\partial v}{\partial z} + \frac{uv^2}{r} + \frac{v^2}{r}\frac{\partial u}{\partial r}$

Azimuthal Momentum Equation:

$$u\frac{\partial v}{\partial r} + \frac{uv}{r} + w\frac{\partial v}{\partial z} = \nu\nabla^2 u - \beta_1 M_\theta - \frac{\sigma B_0^2}{\rho_f}v - \frac{\nu}{k^*}v - F_r v^2 \quad [3]$$

$$M_\theta = u^2\frac{\partial^2 v}{\partial r^2} + w^2\frac{\partial^2 v}{\partial z^2} + 2uw\ \frac{\partial^2 v}{\partial r\partial z} + \frac{2uv}{r}\frac{\partial u}{\partial r} + \frac{2vw}{r}\frac{\partial u}{\partial z} - \frac{2u^2 v}{r} - \frac{v^3}{r^2} + \frac{v^2}{r}\frac{\partial v}{\partial r}$$

Energy Equation (Cattaneo–Christov Form):

$$u\frac{\partial T}{\partial r} + w\frac{\partial T}{\partial z} = \alpha_m\nabla^2 T + D_B\nabla T - \nabla \mathrm{C} + \frac{D_T}{T_\infty}|\nabla T|^2 + \frac{D_k T}{C_s C_p}\nabla^2 C - \lambda_2 H + q^* \quad [4]$$

Where $H = \left(u^2\frac{\partial^2 T}{\partial r^2} + w^2\frac{\partial^2 T}{\partial z^2} + 2uw\frac{\partial^2 T}{\partial r\partial z} + \left(u\frac{\partial u}{\partial r} + w\frac{\partial u}{\partial z}\right)\frac{\partial T}{\partial r} + \left(u\frac{\partial w}{\partial r} + w\frac{\partial w}{\partial z}\right)\frac{\partial T}{\partial z}\right)$

$$q^* = \frac{k_\infty U_w}{z\nu(\rho c)_f}\{A^*(T_w - T_\infty)f + B^*(T - T_\infty)\} \quad [5]$$

Concentration Equation :

$$u\frac{\partial C}{\partial r} + w\frac{\partial C}{\partial z} = D_B\nabla^2 C + \frac{D_T}{T_\infty}\nabla^2 T + \frac{D_k T}{T_m}\nabla^2 T - k_r^2(C - C_\infty)\left(\frac{T}{T\infty}\right)^2 Exp\left(-\frac{E_a}{KT}\right) \quad [6]$$

Where in all the above equations cylindrical Laplacian is

$$\nabla^2=\left(\frac{\partial^2 u}{\partial r^2}+\frac{1}{r}\frac{\partial u}{\partial r}-\frac{u}{r^2}+\frac{\partial^2 u}{\partial z^2}\right)$$

The velocity components are represented by the axes u, v, and w along with the axis $r, \phi \; and \; z$ Axis respectively. The fluid temperature T, the concentration of nanoparticles C, and the kinematic viscosity of the fluid are ν_f, ρ_f is the density of the fluid, α_m is the thermal diffusivity, τ, for the capacity of nanoparticles,λ_2 is the thermal relaxation factor, q^* is the non-uniform heat source/sink term, A^*, B^* are source and sink coefficients, respectively.D_T, D_B are Brownian diffusion & Thermophoresis diffusion, respectively.

The boundary conditions are

$$\left.\begin{array}{c} u=cr, v=r\Omega, w=0, -k\frac{\partial T}{\partial z}=h\left(T_f-T\right), C_w=C \; at \; \eta=0 \\ u\to u_e, v\to 0, T\to T_\infty, \; C\to C_\infty, \eta\to\infty \end{array}\right\} \quad [7]$$

Similarity transformations:

$$\left.\begin{array}{c} u(\eta)=r\Omega F(\eta) v(\eta)=r\Omega G(\eta) w(\eta)=\sqrt{\Omega\nu}\, H(\eta) \eta=\sqrt{\frac{\Omega}{\nu}}\, z \\ \theta(\eta)=\frac{T-T_\infty}{T_f-T_\infty}\varphi(\eta)=\frac{C-C_\infty}{C_w-C_\infty} \end{array}\right\} \quad [8]$$

Equation (8) into equation (1),(2),(3),(4),(5)& (6),

We have

$$H'+2F=0 \quad [9]$$

$$F''(1+\varpi H^2)-F^2+G^2-HF'-2\varpi(FF'H-GG'H)-\varepsilon^2-M(\varepsilon-F)-K(\varepsilon-F)-Fr(\varepsilon-F^2)=0 \quad [10]$$

$$G''(1+\varpi H^2)-2FG-HG'-2\varpi(FG'H+F'GH)-MG-KG-FrG^2=0 \quad [11]$$

$$\theta''+P_r(N_b\theta'\phi'+N_t\theta'^2-H\theta'+\gamma_1(H^2\theta''+HH'\theta')+AH+B\theta+Du\phi'')=0 \quad [12]$$

$$\phi''+\frac{N_t}{N_b}\theta''+ScSr\theta''-ScH\phi'-R\,Sc(1+\delta\theta)^n Exp\left(\frac{-E}{(1+\delta\theta)}\right)=0 \quad [13]$$

Equation (8) into equation (7), we have

Boundary conditions are transformed into

$$\left.\begin{array}{c} F(0)=1, G(0)=\varpi, H(0)=0, \theta'(0)=-Bi+Bi\left(\theta(0)\right) \\ F(\infty)\to\varepsilon, G(\infty)\to 0, \theta(\infty)\to 0, \phi(\infty)\to 0 \end{array}\right\} \quad [14]$$

The dimensionless quantities indicated by the velocity ratio parameter $\varepsilon=\frac{d}{c}$, Deborah parameter $\varpi=\beta_1\Omega$, Porosity parameter $K=\frac{\vartheta}{k^*\Omega}$, Magnetic parameter $M=\frac{\sigma B_0^2}{\rho_f\Omega}$, Forchhiemer parameter $Fr=\Omega F_r$, Prandtl number $P_r=\frac{\vartheta}{\alpha_m}$,$\gamma_1=4\lambda_2\Omega$ for the Thermal relaxation time, $A=A^*\left(\frac{k_\infty U_w}{z\nu(\rho c)_f}\right)$, $B=B^*\left(\frac{k_\infty U_w}{z\nu(\rho c)_f}\right)$ are represented as space, temperature-dependent heat generation and absorption parameters, respectively, Soret number $Sr=\frac{Dk_T}{T_m\vartheta}\left(\frac{T_w-T_\infty}{C_w-C_\infty}\right)$, Brownian motion parameter $N_b=\frac{\tau D_B}{\vartheta}(C_w-C_\infty)$, Thermophoresis parameter $N_t=\frac{\tau D_T}{\vartheta T_\infty}(T_w-T_\infty)$, Dufour number $Du=\frac{Dk_T}{C_sC_p\Omega}\left(\frac{C_w-C_\infty}{T_w-T_\infty}\right)$, Schmidt number $Sc=\frac{\vartheta}{D_B}$, $R=K_r^2$ chemical reaction parameter, $\delta=\frac{T_{f-}T_\infty}{T_\infty}$ temperature ratio parameter, $E=\frac{E_a}{KT_\infty}$ stretching ratio parameter.

$C_F$drag force number, Nu_r Nusselt number Sh_r Sherwood numbers are reduced as below.

$$\left.\begin{array}{c} C_FRe_r^{0,5}=[F'^2(0)+G'^2(0)]^{0.5} \\ Nu_rRe_r^{-0.5}=-\theta'(0) \\ Sh_rRe_r^{-0.5}=-\phi'(0) \end{array}\right\} \quad [15]$$

Where Re_r is the local Reynolds $Re_r=\frac{ru_w}{v}$

3. Results and Discussion

Figures 1 to 3: The Deborah number ϖ is shown in Figure.1 & Figure 2 as a representation of the changes in its relaxation time depending on the various parameters of the fluid. The velocity fluid is affected by the Deborah numberϖ, which decreases in radial velocity $F(\eta)$ and azimuthal velocity$G(\eta)$. Figure 3 shows that the Deborah number ϖ effects on the axial velocity$H(\eta)$. It shows that an increment in the ϖ increases the axial velocity $H(\eta)$.

Figure 4 indicates that the magnetic parameter M on radial velocity $F(\eta)$. The Maxwell Nanofluid particles significantly decrease as the magnetic parameter M values enhancement. This physical phenomenon can be maintained by the reduction in its liquid motion as the Lorentz forces appear.

In Figures 5 & 6, it shows that as the magnetic variable M increases, the disk's concentration & temperature profiles also decrease in azimuthal velocity $G(\eta)$ and axial velocity $H(\eta)$.

Figure 7:The figure indicates that the distinct Fr values are displayed through the distinct curves. If Fr increases, the radial velocity profile F(η) decreases more rapidly.

Figure 8:The plots indicate that the tangential velocity $G(\eta)$ decreases as Fr increases. Reduced tangential velocity $G(\eta)$ at the surface is shown in the Figure. The slope of the curve decreases, caused by different values of Fr. For larger values of η, the tangential velocity approaches zero and falls further from the surface, which is consistent with boundary layer behavior.

Figure 9:If Fr increases, the axial velocity $H(\eta)$decreases. In other words, as Fr increases, the rate of axial velocity decreases relative to the acceleration.

Figures 10 to 12. The increment in the porosity parameter K, as shown in Figures.11 &12, respectively, illustrates that the changes in the speed at which the fluid moves in azimuthal velocity $G(\eta)$ and axial velocity $H(\eta)$ are observed, and that the liquid's speed increases, then its boundary layer's thickness is decreased. Figure 10: The radial velocity $F(\eta)$ In the opposite direction, the flow becomes slower due to the presence of a thin area.

The influence of the rotation parameter ω on the radial velocity $F(\eta)$ and its behavior is shown in Figure 13. The movement of the fluid particles is caused by the centrifugation force, which amplifies the radial velocity$F(\eta)$. When the rotation parameter exceeds the extension, the radial velocity is greater than that of the disc at the surface, where it displays expansion. According to the study, the influence of rotating forces on the surface of the disk is limited. It eventually disappears.

The influence of the rotation parameter on the tangential velocity of the boundary layer is shown in Figure.14. If the rotational parameter increases, the velocity of the boundary layer thickness increases in amplitude. The physical explanation is that the disk's rotation causes the tangential velocity $G(\eta)$ to increase.

The study also noted that the rotation parameter ω impact on the surface of the disk is minimal as one moves away from the boundary layer. As its value increases, the fluid's axial velocity $H(\eta)$ goes up in the z-axis' negative direction as shown in Figure 15.

The Prandtl number's influence Pr on the value of $\theta(\eta)$as shown in Figure 16, although its accuracy increases, and the Prandtl number Pr decreases as its thermal diffusivity increases. As its Prandtl number grows, its temperature gradually decreases.

Effects of chemical reaction parameter R on temperature distribution $\theta(\eta)$ The distribution and concentration profile $\phi(\eta)$ is shown in the Figures. 17 & 18. It is clear that an increase in the chemical reaction parameter increases the temperature profile and decreases the concentration profile.

Figures 19 & 20 show similar correlations between the thermal field and the concentration distribution $\phi(\eta)$ in Nb. The level of the thermophiles factor's correlation with the dimensionless heat variable is shown in the same manner. It indicates that these parameters can improve the disk's thermal performance. The enhanced thermal performance of the disk is explained by the mechanisms by which the additional heat is able to expand the flow of heat from the surface of the disc.

The concentration distribution $\phi(\eta)$ Nb's features are also studied in the concentration distribution. Nb's features are also studied in Figure 20. The level of the thermophoresis factor's correlation with the dimensionless thermal variable Nb shows that the higher the amount of this factor, the better the thermal performance of the disk. This is because the additional heat that is generated from the surface of the disc is able to expand the flow of heat.

The figure 21 illustrates the influence of the heat source parameter A on the temperature distribution $\theta(\eta)$ within the thermal boundary layer. It is observed that increasing A enhances the temperature profile throughout the boundary layer region.

Figure 22 illustrates the variation of the temperature profile $\theta(\eta)$ for the different values of source parameter A. If the source parameter A is increasing, the profiles slightly decrease and decay more rapidly toward zero, and it is indicating that the thermal boundary layer thickness reduces.

Figure 23 & 24 state that the Soret number Sr shows how the temperature gradient's influence can affect the concentration field$\phi(\eta)$. High Soret numbers can lead to more concentration dispersion due to increased convective flow. It should be noted that Soret numbers have different effects on the concentration field $\phi(\eta)$ and temperature field$\theta(\eta)$. For instance, as the boundary layer's thickness increases, its heat transmission and mass transmission rates go up.

Figure 25. The lower the number Du on the temperature profile$\theta(\eta)$, the greater the temperature difference between the free stream fluid and the wall. This causes the fluid to absorb less heat, and thus its viscosity increases.

Figure 26. It is noted that a rise in the temperature can be triggered by the increase in Du. The concentration profile $\phi(\eta)$ gradient's impact on temperature can be strengthened by Dufour. It can then promote thermal energy and flows within the region, which can lead to a significant increase in its thickness.

As shown in Figure 27, the value of Bi increases as the temperature profile $\theta(\eta)$ rises, and this leads to a significant increase in the boundary layer's thickness. Therefore, the rate increase was affected by the Bi value present.

Figure 28 depicts the effect of the thermal relaxation parameter on the temperature profile θ(η). It is evident that increasing the thermal relaxation coefficient reduces the temperature distribution within the boundary layer. Physically, the Cattaneo–Christov heat flux model introduces a finite speed of heat propagation through the thermal relaxation time parameter. As this parameter increases, the heat conduction process is delayed, weakening thermal diffusion and consequently lowering the fluid temperature. This behavior reflects the non-Fourier heat transfer mechanism and its insulating tendency within the system.

4. Conclusion

The researchers studied the flow dynamics of a Maxwell nanofluid with a spinning disk and a shrinking disk. They also looked into its temperature and the impact of sink or heat source on its flow behavior and concentration fields. Through their study, the researchers were able to identify the important features of the Nusselt number and the fluid temperature.

- The velocity outline decreases as the Deborah number ϖ increases.
- The researchers noticed a rise in the magnetic factors when the velocity profile $f(\eta)$ decreased.
- Although the Nb parameter's increase led to a positive temperature profile$\theta(\eta)$, this trend reversed after a while.
- The values of M and εparameters increased, causing the Sherwood number and skin friction factor to follow suit.

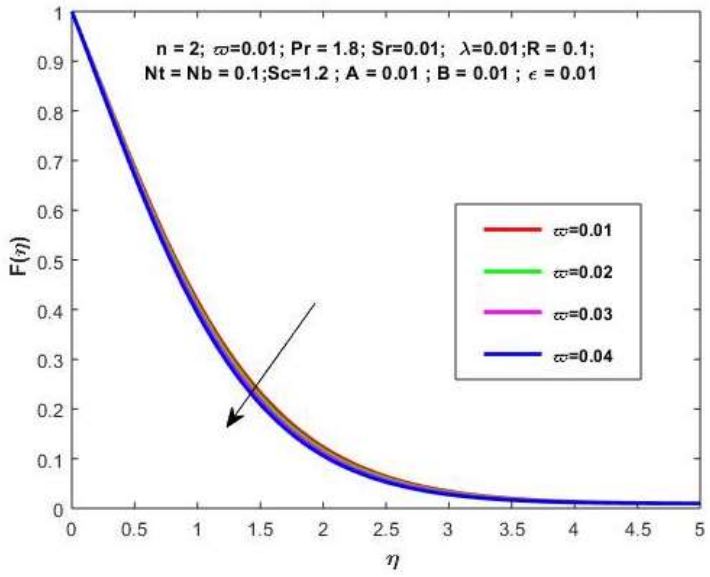

Fig. 1 Effect of Deborah number ϖ on $F(\eta)$.

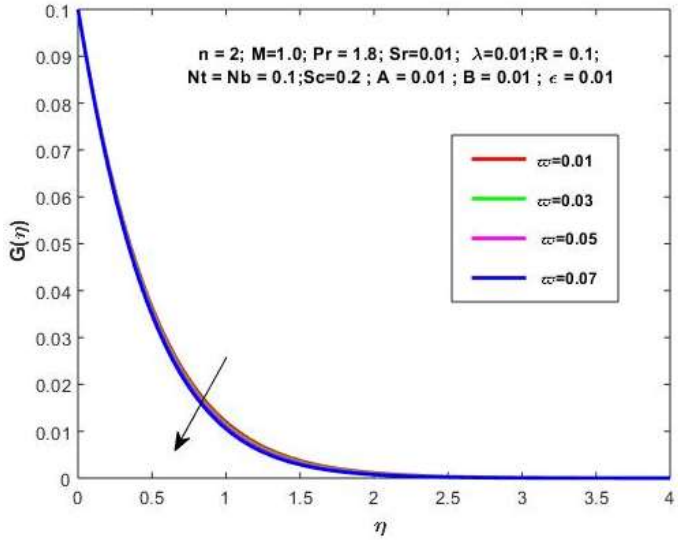

Fig. 2 Effect of Deborah number ϖ on $G(\eta)$.

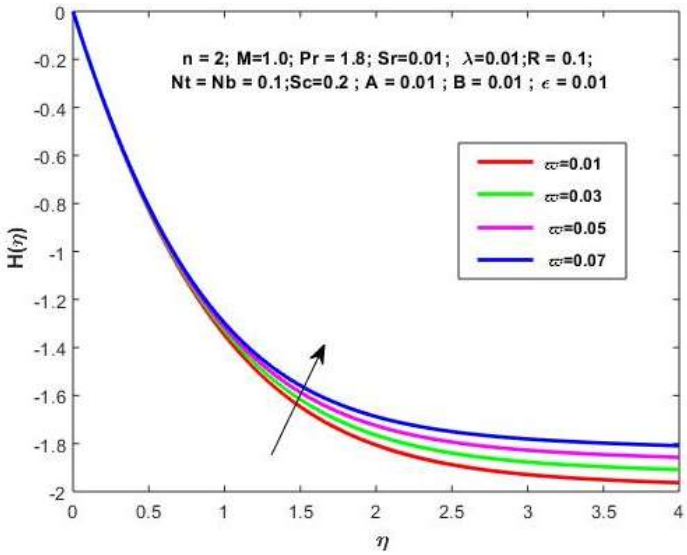

Fig. 3 Effect of Deborah number ϖ on $H(\eta)$.

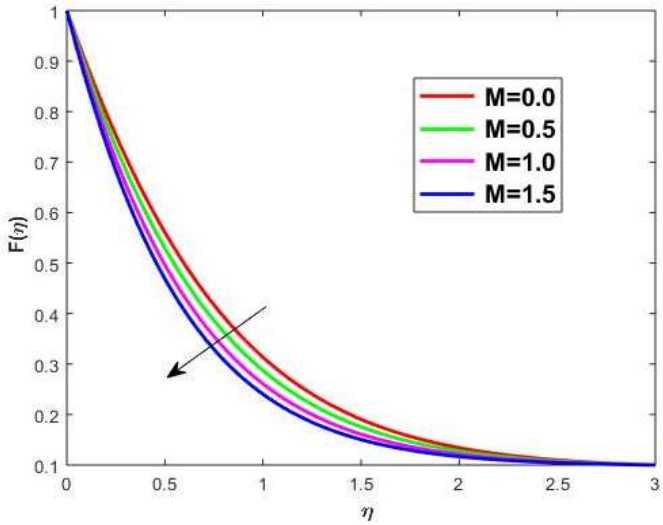

Fig. 4 Various of Magnetic parameter M on radial velocity $F(\eta)$.

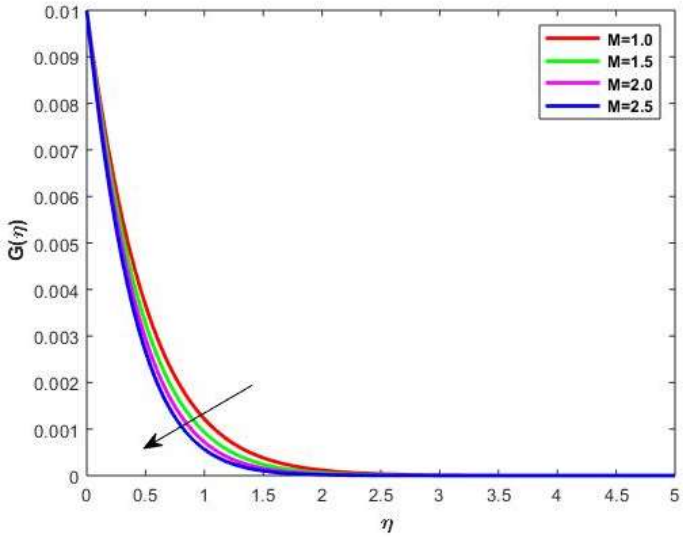

Fig. 5 Various of Magnetic Parameters M on Tangential velocity $G(\eta)$

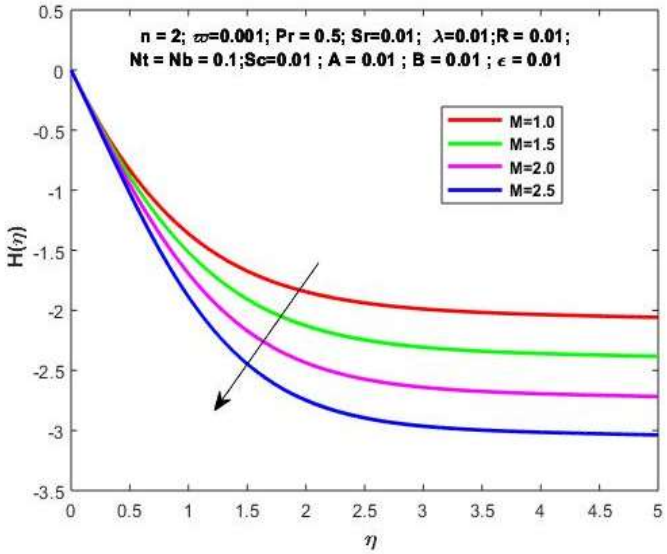

Fig. 6 Various of Magnetic parameter M on axial velocity $H(\eta)$.

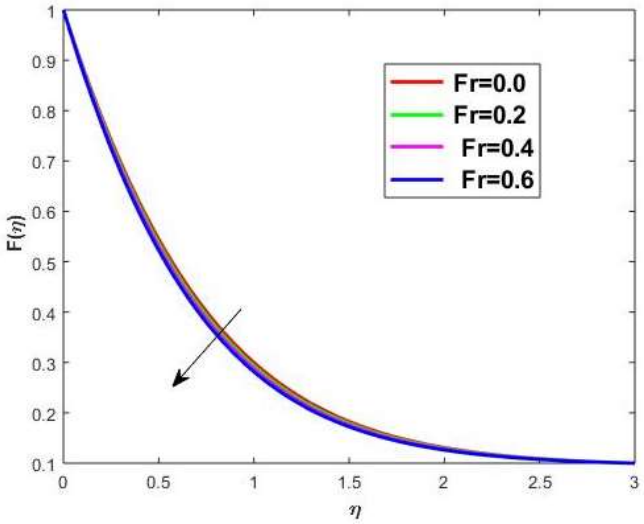

Fig. 7 Effects of Fr on radial velocity $F(\eta)$.

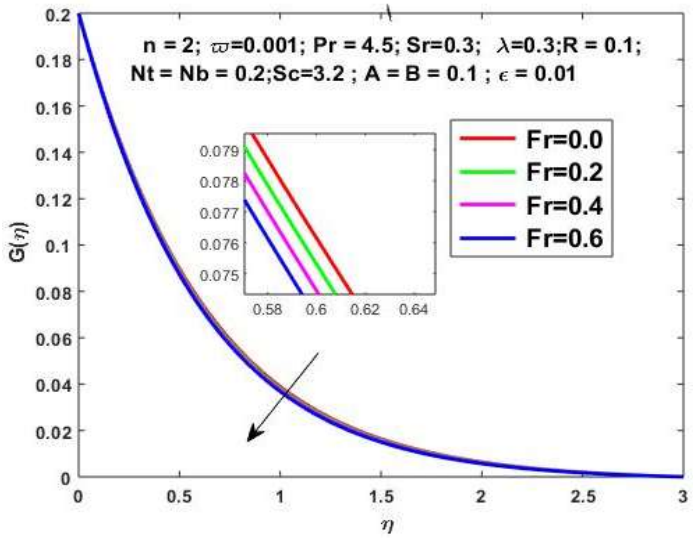

Fig. 8 Effects of Fr on Tangential Velocity

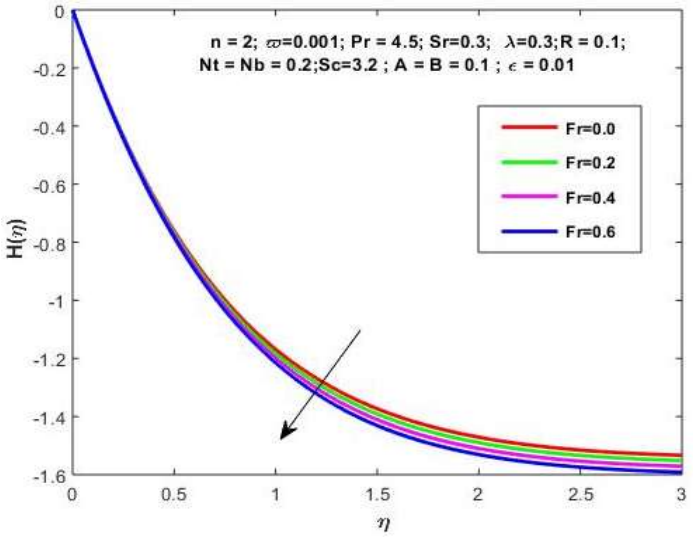

Fig. 9 Effects of Fr on axial velocity $H(\eta)$.

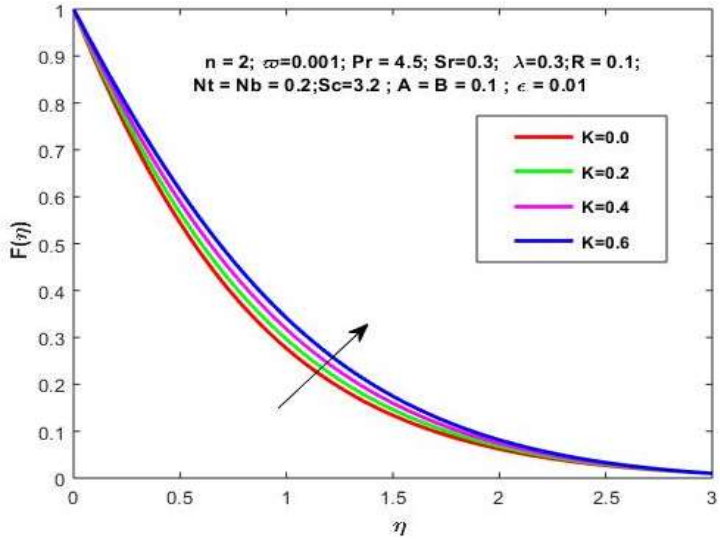

Fig. 10 Effects of K on radial velocity$F(\eta)$.

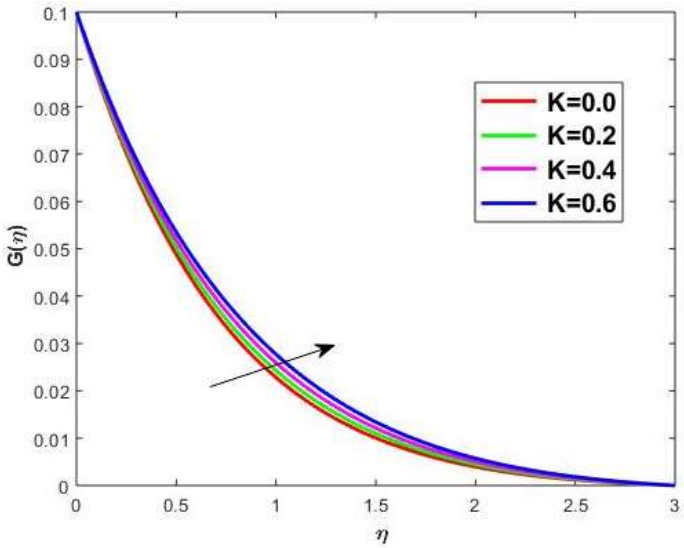

Fig. 11 Effects of K on tangential velocity $G(\eta)$

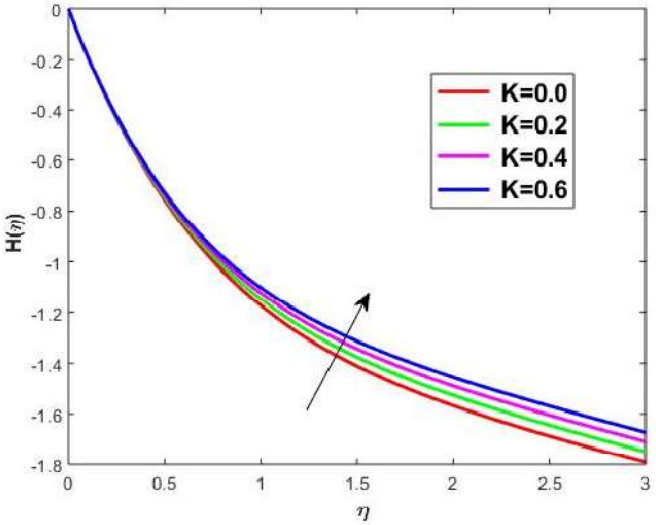

Fig. 12 Effects of K on axial velocity H(η).

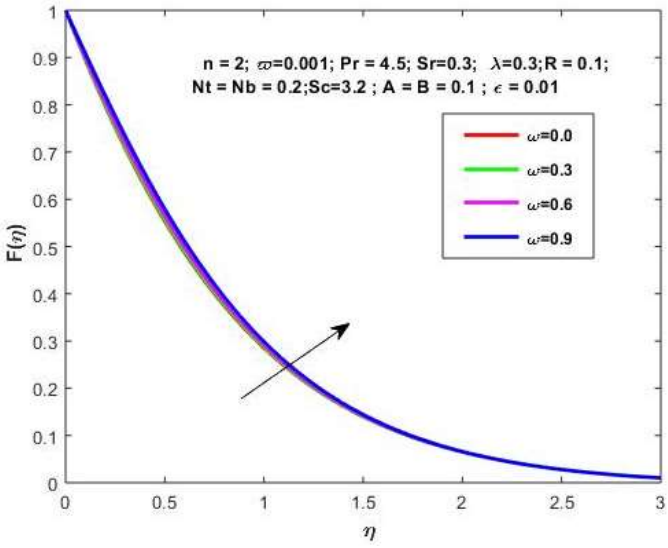

Fig. 13 Effects of ω on $F(\eta)$.

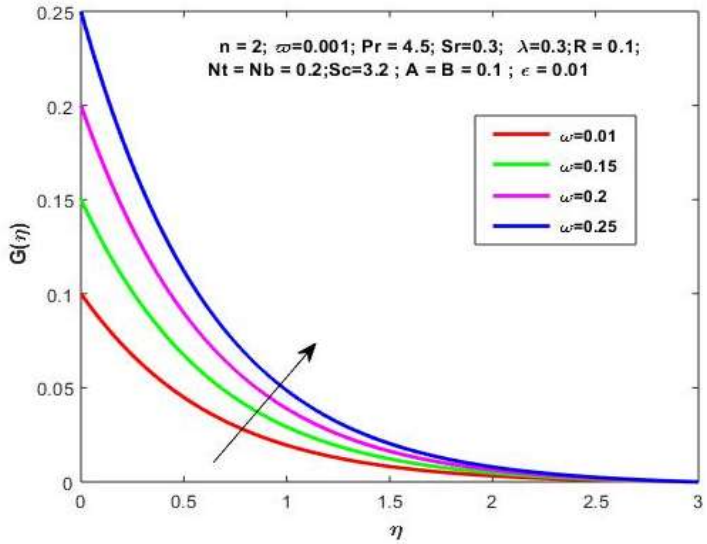

Fig. 14 Effects of ω on $G(\eta)$

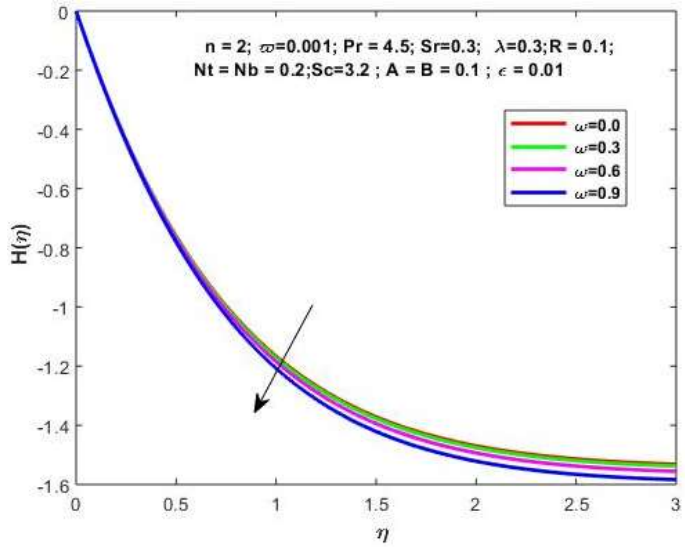

Fig. 15 Effects of ω on $H(\eta)$.

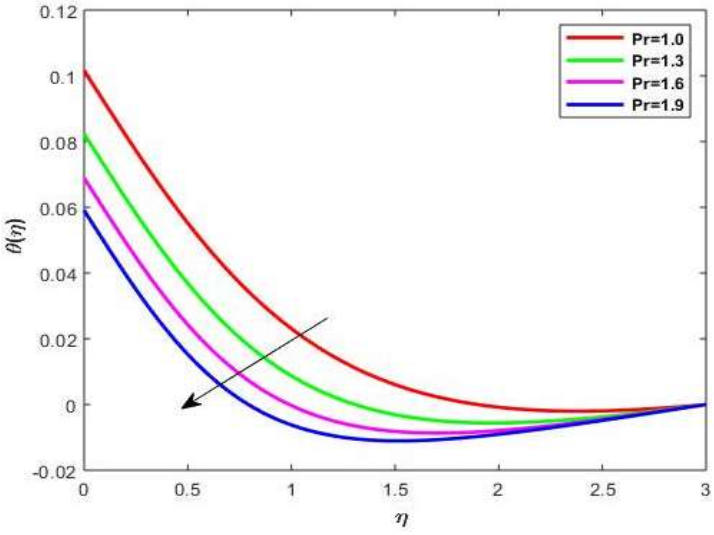

Fig. 16 Effects of Pr on $\theta(\eta)$.

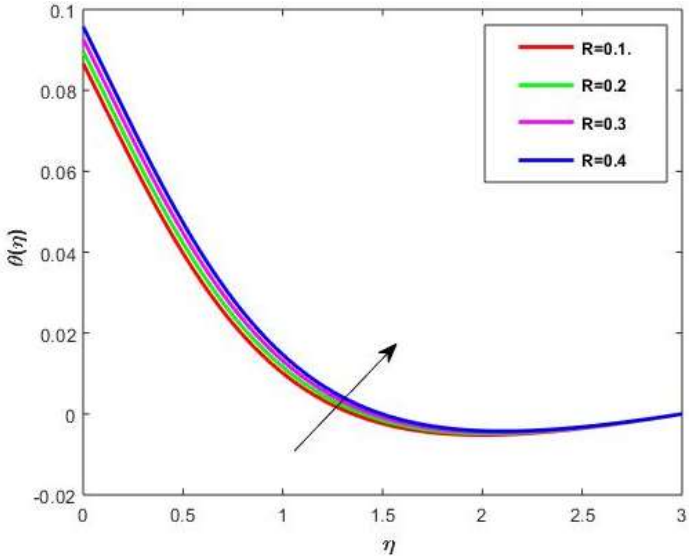

Fig. 17 Effects of R on $\theta(\eta)$.

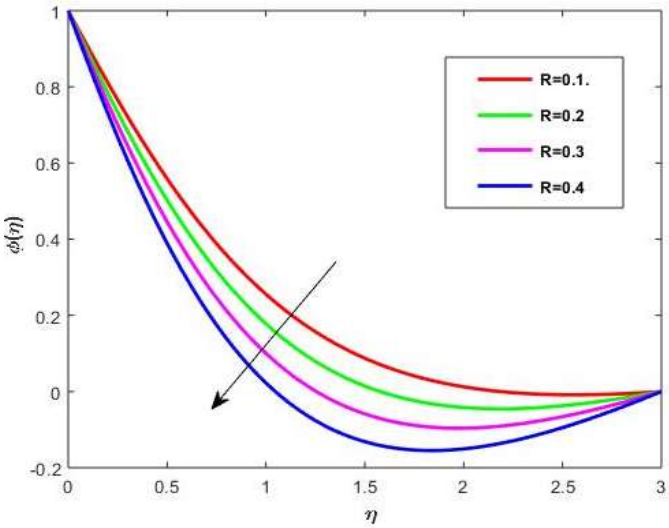

Fig. 18 Effects of R on $\phi(\eta)$.

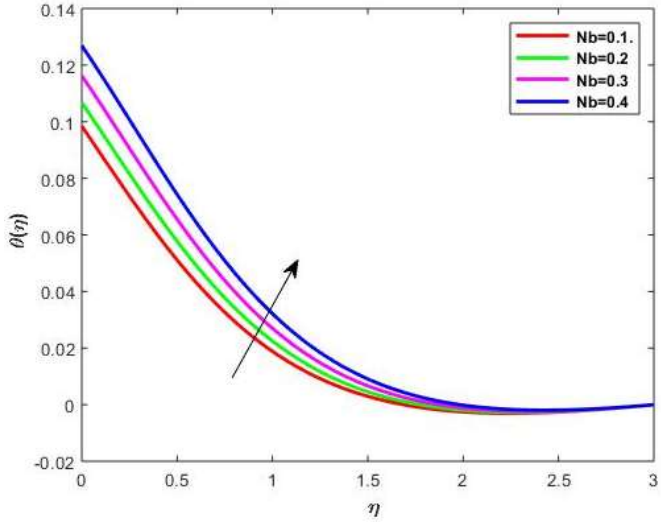

Fig. 19 Effects of Nb on $\theta(\eta)$.

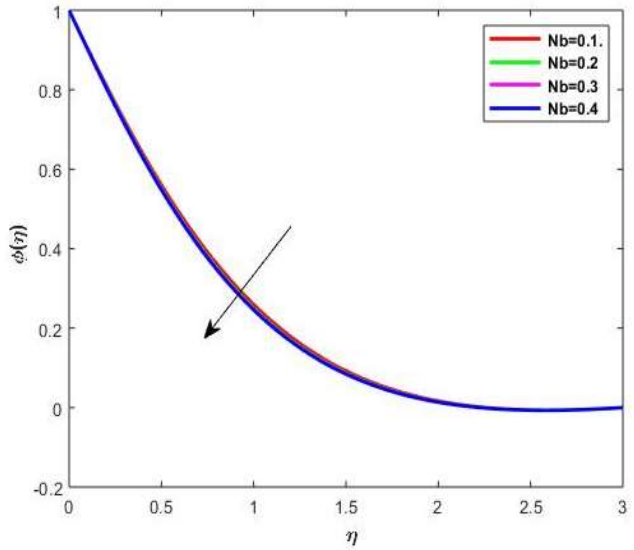

Fig. 20 Effects of Nb on $\phi(\eta)$.

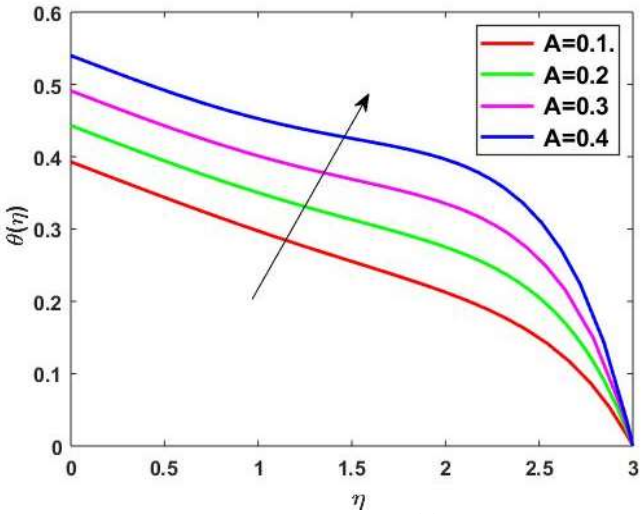

Fig. 21 Effects of A on $\theta(\eta)$.

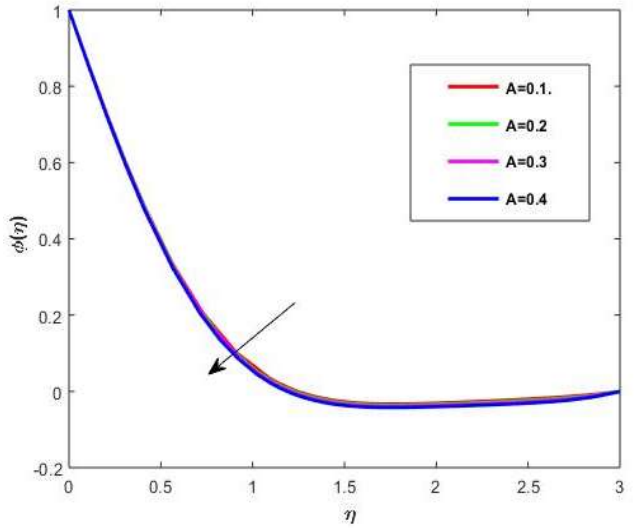

Fig. 22 Effects of A on $\phi(\eta)$.

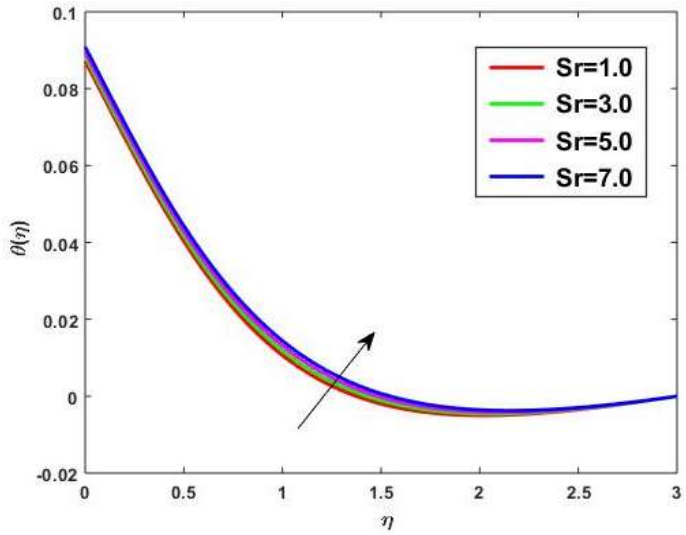

Fig. 23 Effects of Sr on $\phi(\eta)$

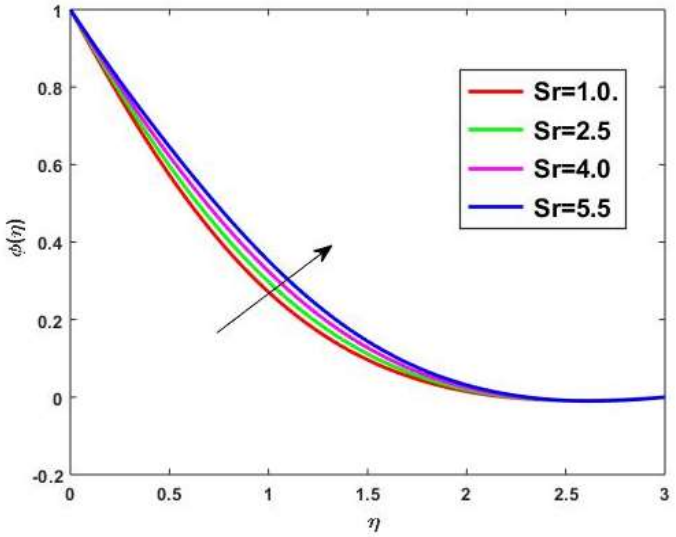

Fig. 24 Effects of Sr on $\theta(\eta)$

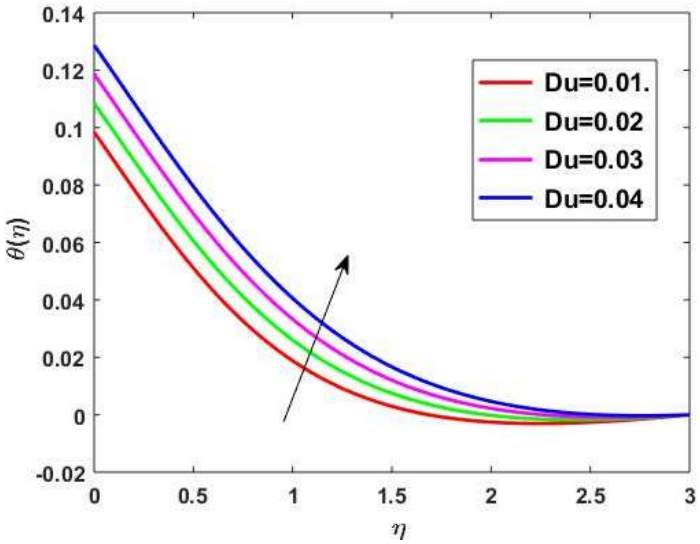

Fig. 25 Effects of D_u on $\phi(\eta)$

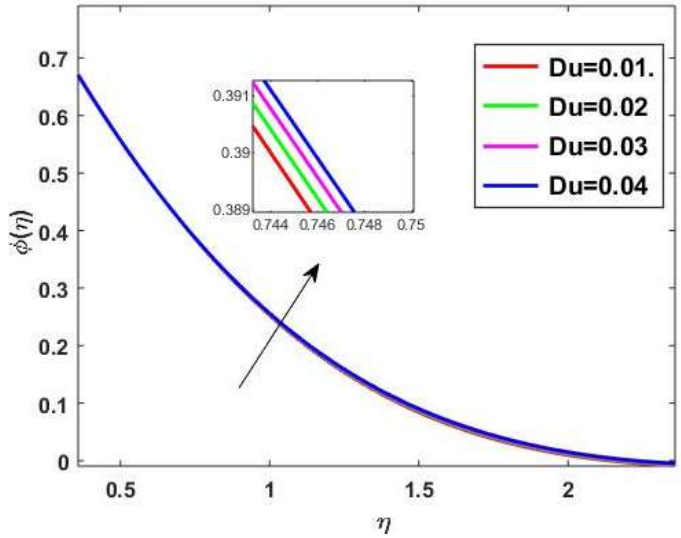

Fig. 26 Effects of Du on $\theta(\eta)$.

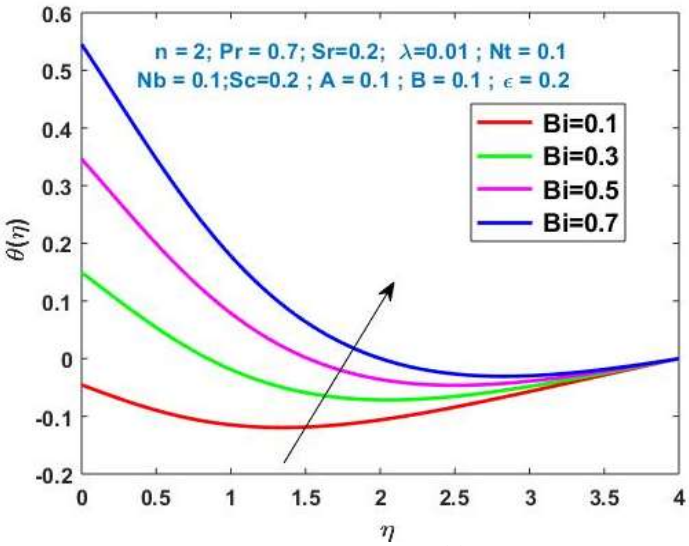

Fig. 27 Effects of Bi on $\theta(\eta)$

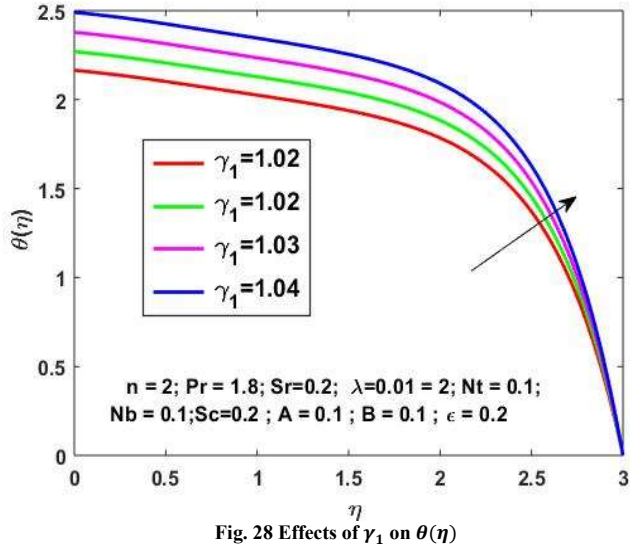

Fig. 28 Effects of γ_1 on $\theta(\eta)$

Table 1. Results of the computational of skin friction $Cf_r Re_r^{0.5}$ for the various values $M, \varpi, \epsilon, \omega$, Fr, K as shown in the table below

M	ϖ	ϵ	ω	Fr	K	$Cf_r Re_r^{0.5}$
0.1	0.01	0.1	0.1			1.157067
0.2						1.130035
0.3						1.102585
0.4						1.074745
	0.01					0.911139
	0.02					0.920595
	0.03					0.930044
	0.04					0.939482
		0.1				0.902628
		0.2				0.967022
		0.3				1.064254
		0.4				1.215504
			0.1			0.737907
			0.2			0.803539
			0.3			0.902628
			0.4			1.025833
				0.0		0.904328
				0.2		0.870684
				0.4		0.837992
				0.6		0.806591
					0.0	0.916241
					0.2	0.858925
					0.4	0.804097
					0.6	0.750166

Table 2. Comparing of $f'(0), g'(0)$ and $\theta(0)$ for the values $M = 0.5$ and $Pr = 0.7$

	Yin et al (2017)	Present
$f'(0)$	0.51020	0.5102212
$g'(0)$	0.6159	0.6159120

References

[1] TH. Von Karman, "Uber Laminar and Turbulent Reibung," *Journal of Applied Mathematics and Machanics*, vol. 1, no. 4, pp. 233-255, 1921. [CrossRef] [Google Scholar] [Publisher Link]

[2] W.G. Cochran, "The Flow Due to a Rotating Disk," *Mathematical Proceedings of the Cambridge Philosophical Society*, vol. 30, no. 3, pp. 365-375,1934. [CrossRef] [Google Scholar] [Publisher Link]

[3] S. Goldstein, "On the Resistance to the Rotation of a Disc Immersed in a Fluid," *Mathematical Proceedings of the Cambridge Philosophical Society*, vol. 31, no. 2, pp. 232-241, 1935. [CrossRef] [Google Scholar] [Publisher Link]

[4] N. Gregory, John Trevor Stuart, and W.S. Walker, "On the Stability of Three-Dimensional Boundary Layers with Application to the Flow Due to a Rotating Disk," *Philosophical Transactions A*, vol. 248, no. 943, pp. 155-199, 1955. [CrossRef] [Google Scholar] [Publisher Link]

[5] P. Sibanda, and O.D. Makinde, "On Steady MHD Flow and Heat Transfer Past a Rotating Disk in a Porous Medium with Ohmic Heating and Viscous Dissipation," *International Journal of Numerical Methods Heat Fluid Flow*, vol. 20, no. 3, pp. 269-285, 2010. [CrossRef] [Google Scholar] [Publisher Link]

[6] K. Hiemenz, "The Boundary Layer on a Straight Circular Cylinder Immersed in a Uniform Liquid Flow," *Dinglers Polytechnisches Journal*, vol. 326, pp. 321-324, 1911. [Google Scholar]

[7] F. Homann, "The Influence of High Viscosity on the Flow around a Cylinder and a Sphere," *Journal of Applied Mathematics and Machanics*, vol. 16, no. 3, pp. 153-164, 1936. [CrossRef] [Google Scholar] [Publisher Link]

[8] C.Y. Wang, "Stagnation Flow on the Surface of a Quiescent Fluid - An Exact Solution of the Navier- Stokes Equations," *Quarterly of Applied Mathematics*, vol. 43, pp. 215-223, 1985. [CrossRef] [Google Scholar] [Publisher Link]

[9] T. Hayat et al., "Newtonian Heating in Stagnation Point Flow of Burgers Fluid," *Applied Mathematics and Mechanics*, vol. 36, pp. 61-68, 2015. [CrossRef] [Google Scholar] [Publisher Link]

[10] H.L. Agrawal, "A New Exact Solution of the Equations of Viscous Motion with Axial Symmetry," *The Quarterly Journal of Mechanics and Applied* Mathematics, vol. 10, no. 1, pp. 42-44, 1957. [CrossRef] [Google Scholar] [Publisher Link]

[11] Patrick Weidman, "Axisymmetric Rotational Stagnation-Point Flowimpinging on a Rotating Disk," *Journal of Applied Mathematics and Physics*, vol. 66, pp. 3425-3431, 2015. [CrossRef] [Google Scholar] [Publisher Link]

[12] Mustafa Turkyilmazoglu, "Analytical Solutions of Single and Multi-Phase Models for the Condensation of Nanofluid Film Flow and Heat Transfer," *European Journal of Mechanics-B/Fluids*, vol. 53, pp. 272-277, 2015. [CrossRef] [Google Scholar] [Publisher Link]

[13] Y.Y. Lok, J.H Merkin, and I. Pop, "Axisymmetric Rotational Stagnation-Point Flow Impinging on a Permeable Stretching/Shrinking Rotating Disk," *European Journal of Mechanics - B/Fluids*, vol. 72, pp. 275-292, 2018. [CrossRef] [Google Scholar] [Publisher Link]

[14] M. Sajid et al., "Numerical Simulation for Homann Flow of Amicropolar Fluid on a Spiraling Disk," *European Journal of Mechanics - B/Fluids*, vol. 72, pp. 320-327, 2018. [CrossRef] [Google Scholar] [Publisher Link]

[15] Stephen Whitaker, "Flow in Porous Media I: A Theoretical Derivation of Darcy's Law," *Transport in Porous Media*, vol. 1, pp. 3-25, 1986. [CrossRef] [Google Scholar] [Publisher Link]

[16] M. Muskat, "The Flow of Homogeneous Fluids through Porous Media," *Soil Science*, vol. 46, no. 2, 1938. [Google Scholar] [Publisher Link]

[17] Tasawar Hayat et al., "FDM Analysis for Nonlinear Mixed Convective Nanofluid Flow with Entropy Generation," *International Communications in Heat and Mass Transfer*, vol. 126, 2021. [CrossRef] [Google Scholar] [Publisher Link]

[18] M. Adil Sadiq et al., "Partial Slip in Darcy-Forchheimer Carbon Nanotubes Flow by Rotating Disk," *International Communications in Heat and Mass Transfer*, vol. 116, 2020. [CrossRef] [Google Scholar] [Publisher Link]

[19] Taseer Muhammad et al., "Darcy-Forchheimer Flow Over an Exponentially Stretching Curved Surface with Cattaneo-Christov Double Diffusion," *Physica A Statistical Mechanics and its Applications*, vol. 556, 2020. [CrossRef] [Google Scholar] [Publisher Link]

[20] Farwa Haider, Tasawar Hayat, and Ahmed Alsaedi, "Flow of Hybrid Nanofluid through Darcy-Forchheimer Porous Space with Variable Characteristics," *Alexandria Engineering Journal*, vol. 60, no. 3, pp. 3047-3056, 2021. [CrossRef] [Google Scholar] [Publisher Link]

[21] C. Cattaneo, "On Heat Conduction," *Atti Del Seminario Matematico e Fisico Dell'università di Modena*, vol. 3, pp. 83-101, 1948. [CrossRef] [Google Scholar] [Publisher Link]

[22] Tasawar Hayat et al., "Flow Between Two Stretchable Rotating Disks with Cattaneo-Christov Heat Flux Model," *Results in Physics*, vol. 7, pp. 126-133, 2017. [CrossRef] [Google Scholar] [Publisher Link]

[23] S.A. Shehzad et al., "Double-Diffusive Cattaneo–Christov Squeezing Flow of Micropolar Fluid," *Journal of Thermal Analysis and Calorimetry*, vol. 143, pp. 445-454, 2021. [CrossRef] [Google Scholar] [Publisher Link]

[24] A. Bhattacharyya et al., "Simulation of Cattaneo-Christov Heat Flux on the Flow of Single and Multi-Walled Carbon Nanotubes between Two Stretchable Coaxial Rotating Disks," *Journal of Thermal Analysis and Calorimetry*, vol. 139, no. 3, pp. 1655-1670, 2020. [CrossRef] [Google Scholar] [Publisher Link]

[25] Ayele Tulu, and Wubshet Ibrahim, "MHD Slip Flow of CNT-Ethylene Glycol Nanofluid Due to a Stretchable Rotating Disk with Cattaneo–Christov Heat Flux Model," *Mathematical Problems in Engineering*, vol. 20, pp. 1-13, 2020. [CrossRef] [Google Scholar] [Publisher Link]

[26] Sachin Shaw, "Impact of Cattaneo–Christov Heat Flux on Al_2O_3–Cu/H_2O–$(CH_2OH)_2$ Hybrid Nanofluid Flow between Two Stretchable Rotating Disks," *Energy Systems and Nanotechnology*, pp. 329-368, 2021. [CrossRef] [Google Scholar] [Publisher Link]

[27] Ziya Uddin et al., "Wubshet Ibrahim Particle Swarm Optimization for Exploring Darcy-Forchheimer Flow of Casson Fluid Between Co-Axial Rotating Disks with the Cattaneo-Christov Model," *Scientific Reports*, vol. 13. pp. 78-91, 2024. [CrossRef] [Google Scholar] [Publisher Link]

[28] Sobia Noreen et al., "Comparative Study of Ternary Hybrid Nanofluids with Role of Thermal Radiation and Cattaneo-Christov Heat Flux between Double Rotating Disks," *Scientific Reports*, vol. 13, pp. 77-95, 2023. [CrossRef] [Google Scholar] [Publisher Link]

[29] N. Pothanna et al., "Unsteady Thermo-Viscous Fluid Motion Between Two Infinitely Extended Impermeable Horizontal Plates — An Artificial Neural Networks Approach," *Thermal Science and Engineering Progress*, vol. 62, 2025. [CrossRef] [Google Scholar] [Publisher Link]

[30] Pothanna Nalimela et al., "Artificial Neural Networks Analysis of an Unsteady Fluid Flow through a Horizontal Oscillating Flat Plate in a Porous Slab," *Physics of Fluids*, vol. 37, no. 2, 2025. [CrossRef] [Google Scholar] [Publisher Link]

[31] N. Pothanna, "Investigation on Unsteady Fluid Flow around an Oscillating Sphere — A Numerical and Analytical Approach," *Hybrid Advances*, vol. 6, pp. 1-9, 2024. [CrossRef] [Google Scholar] [Publisher Link]

[32] N. Pothanna et al., "An Analytical Investigation of Thermo-Viscous Unsteady Fluid Motion Surrounding an Oscillating Sphere," *Results in Engineering*, vol. 27, pp. 1-9, 2025. [CrossRef] [Google Scholar] [Publisher Link]

[33] Swetha Boppani et al., "Numerical Investigation of a Bio-Convective Couple Stress Cnts/Human Blood Hybrid Nanofluid Flow through a Squeezing Channel with Chemical Reaction: A Comparative Study," *Proceedings of the Institution of Mechanical Engineers, Part C: Journal of Mechanical Engineering Science*, vol. 239, no. 22, pp. 9204-9217, 2025. [CrossRef] [Google Scholar] [Publisher Link]

[34] Sandeep Raj Lanka, Ramakrishna Gannarapu, Pothanna Nalimela, "A Study on Effect of Melt Fraction Relaxation Factor in Numerical Simulation with the Enthalpy-Porosity Method for Latent Heat Storage," *Sustainable Chemistry for Climate Action*, vol. 7, pp. 1-13, 2025. [CrossRef] [Google Scholar] [Publisher Link]

[35] P. Raja Shekar, G. Jithender Reddy, and N. Pothanna, "Influence of Thermal Radiation on MHD Casson Nanofluid Flow Over a Nonlinear Stretching Sheet with the Presence of Chemical Reaction," *East European Journal of Physics*, vol. 1, pp. 101-111, 2025. [CrossRef] [Google Scholar] [Publisher Link]

[36] M. Anil Kumar, N. Pothanna, and G. Jithender Reddy, "Analyzing the Heat and Mass Transfer behavior in a 2-D Forchheimer Porous Medium on MHD Casson Fluid Flow Over an Inclined Non-Linear Surface with Viscous Dissipation, Chemical Reaction, and Soret–Dufour Parameters," *Multiscale and Multidisciplinary Modeling, Experiments and Design*, vol. 8, no. 3, 2025. [CrossRef] [Google Scholar] [Publisher Link]

[37] G. Jithender Reddy, P. Mangathai, and N. Pothanna, "Analysis of Heat Generation Impact on Nanofluid Flow over a Stretching Sheet," *Partial Differential Equations in Applied Mathematics*, vol. 11, pp. 1-7, 2024. [CrossRef] [Google Scholar] [Publisher Link]

[38] J. Srinivas et al., "Unsteady Fluid Motion between Infinitely Stretched Parallel Horizontal Plates with the Absence of Viscous Dissipation: An Analytical Approximation," *East European Journal of Physics*, vol. 2, pp. 359-368, 2025. [CrossRef] [Google Scholar] [Publisher Link]

[39] N. Pothanna et al., "Artificial Neural Networks Approach To Analyze Thermo-Viscous Fluid Motion Between Horizontal Porous Stretched Plates Bounded In A Porous Medium," *International Journal of Applied and Computational Mathematics*, vol. 11, 2024. [CrossRef] [Google Scholar] [Publisher Link]